TEM preparation technique influence on an LBM AlSi7Mg0.6 alloy nanostructure

Nicolas Bello, Malo Jullien, Cassiopée Galy, Céline Larignon, Joël Douin

TEM preparation technique influence on an LBM AlSi7Mg0.6 alloy nanostructure

Nicolas Bello[1,2], Malo Jullien[2], Cassiopée Galy[1], Céline Larignon[1] and Joël Douin[2]

[1] IRT Saint Exupéry, B612 - 3 rue Tarfaya - CS34436, 31405 Toulouse Cedex, FR

[2] CEMES, Université de Toulouse, CNRS, 29 rue Jeanne Marvig 31055 Toulouse Cedex 4 FR

Abstract

To provide detailed characteristics on the laser beam melting AlSi7Mg0.6 alloy, transmission electron microscopy is required as the microstructure is composed of aluminum cells hardened by nano-sized precipitates encapsulated in a 3D silicon structure. However, sample preparation techniques can cause local temperature variation or irradiation that impact the local microstructure. With various thin-foil preparations, we have shown that standard twin jet electropolishing produce thin, well-defined aluminum cells filled with nano-sized precipitates. When ion-based methods are used, due to local heating and irradiation, the nanoprecipitates are significantly altered. Lowering the preparation technique temperature appears to be equivalent to twin jet electropolishing.

Keywords: additive manufacturing, Al, Alloy, focused ion beam (FIB), microstructure, phase transformation, transmission electron microscopy (TEM).

Introduction

Laser Beam Melting (LBM) is an additive manufacturing process that produces specific microstructures with high residual stresses as a result of melting, solidification, and fast cooling phenomena that occur much faster than traditional processes. In AlSi7Mg0.6 alloy (wt%) produced by LBM, a 3D $\alpha - Al$ / Si network is formed, with a complex microstructure [1] : a Si-rich cell structure [2–6] surrounding an intracellular $\alpha - Al$ structure that we will focus on. The coexistence of a 3D eutectic network and nanometric-sized precipitates within Al cells, as well as the development of specific additive manufacturing heat treatments in the form of direct artificial aging (i.e., without a solution heat treatment step), has sparked industrial interest in this type of alloy [6]. In our study, one hour of direct artificial aging at 170 °C was performed on AlSi7Mg0.6 alloys. When compared to a conventional T6-type heat treatment consisting of a solution heat treatment followed by artificial aging [7] this heat treatment allows for the preservation of the as-built Si-network and provides good tensile properties.

Similar to other LBMed Al-Si-Mg alloys [8–11], the $\alpha - Al$ phase contains several types of nanoprecipitates (Figure 1). A thorough review of the literature on the techniques used for TEM observations on LBMed alloys revealed some significant differences in microstructure characterization. Some authors used Gatan PIPS systems to prepare AlSi10Mg TEM lamellae and discovered numerous intracellular precipitates [12, 13] that are typically found in aged alloys [14, 15]. This could be caused by the ion beam's high energy. The FIB technique can also be used, but the high energy of the ion beam can lead to microstructural changes because the Ga beam can dissolve some precipitates [16] or increase their size [11]. Some authors use liquid nitrogen with PIPS to reduce local heating but still observe large intracellular precipitates [17, 18].

To better understand the activated hardening mechanisms in this intricate microstructure, a fine characterization of the $\alpha - Al$ phase is required. The aforementioned authors [12–18] investigated the fine precipitation in the $\alpha - Al$ phase of an LBMed AlSi10Mg alloy and discovered no similar or identical nanostructure on the as-built alloy (without any post treatment). It is thus important to determine whether this is due to the elaboration process or to the various preparation techniques. In the present case, we concentrate our efforts on determining the best preparation technique for revealing the most relevant microstructure. The TEM characterization was first carried out on thin foils prepared using a traditional twin jet electropolishing technique, and was completed with dilatometry and differential thermal analyses, as described elsewhere [7]. Then three other preparation techniques were investigated, and the corresponding microstructures of our AlSi7Mg0.6 alloys are presented and compared in this paper.

Materials & Experiments

For this study, an AlSi7Mg0.6 alloy has been transformed by laser beam melting using the parameters described, as well as its chemical composition, in a previous paper [7]. It was then subjected to two post-manufacturing heat treatments: one direct artificial aging and one standard T6-type. Direct Artificial Ageing (DAA) is a one-step heat treatment developed to take advantage of the unique properties of additively manufactured microstructures. Indeed, the heat treatment is defined as a sufficiently low temperature for a short period of time (here 1 hour at 170 °C) to both maintain the as-built organization with Si networks and allow hardening elements to precipitate. As a result, the Si skeleton is preserved, and the $\alpha - Al$ solid solution can be hardened. Another treatment using a solution heat treatment has been developed, the optimized T6 (noted oT6), with the following parameters: solution treatment at 510 °C for 60 minutes with water quenching and artificial aging 170 °C / 240 min, followed by air cooling. The resulting microstructure is then similar to that of the AlSi7Mg0.6-oT6 alloy produced using conventional methods [7].

Prior to using precision ion polishing systems (PIPS) or twin jet electropolishing (TJE), samples were gradually thinned to 20 µm by SiC polishing. After being glued to a copper grid with silver lacquer, PIPS samples were thinned with a GATAN PIPS I at 6 keV / 120 minutes and 3 keV / 10 minutes using Ar ions. TJE samples were thinned in a solution of 2/3 methanol and 1/3 nitric acid with a tension of 40 V at -30 °C and then glued to a copper grid.

Other TEM samples were produced using focused ion beam (FIB) techniques at room temperature (RT) and low temperature (LT). Pt deposition via gas injection systems (GIS) was first performed on the bulk sample surface for both RT-FIB and LT-FIB techniques to protect the sample from the following steps. Then, two cross sections were made apart from the Pt deposition to perform a U-cut lamella. The lamella was then fixed to a copper grid holder with Pt and milled with gradually decreasing energy. Thinning acceleration voltages and currents typically range from 30 kV / 400 pA to 2 kV / 23 pA [8][19]. All FIB millings for the LT-FIB lamella preparation were done at -100 °C, while the Pt deposition was done at room temperature on a FIB-SEM NOVA 200. For RT-FIB lamella preparation, an FEI Helios Nanolab 600i was used.

TEM observations were conducted using a JEOL 2010 HC microscope equipped with a LaB6 filament, operating at an acceleration voltage of 200 kV. All TEM images presented in this study were acquired in the $[001]_{Al}$ direction. These images were captured under bright field conditions, where only the transmitted beam was selected. This technique is widely recognized for defect analysis in a range of materials, including aluminum alloys [20],

titanium alloys [21] and various nanomaterials [22]. It is important to note that all TEM images were deliberately taken in the $[001]_{Al}$ direction to ensure the precise observation of the smallest defects [23].

TEM Characterizations

TEM analysis was performed on samples prepared using twin jet electropolishing and ion-based techniques.

Figure 1 illustrates the fine microstructure of an AlSi7Mg0.6-DAA sample prepared using twin jet-electropolishing. The presence of a continuous Si-rich network forming cells with a 500 nm mean diameter and filled with $\alpha - Al$ characterizes the microstructure.

Because of the local over-thickness of the cell-wall area, the Si-rich network appears darker in the image. Indeed, as shown in Figure 2 a., FEG-SEM analysis of the surface of an AlSi7Mg0.6-DAA sample prepared by twin jet electropolishing reveals selective polishing of the alloy microstructure. The $\alpha - Al$ structure is clearly more affected by the electrolyte, and only the 3D Si structure remains. To compare, the same TJE preparation was carried out on an AlSi7Mg0.6- T6 (Figure 2 b.). TJE causes a selective polishing of the Al-based matrix, revealing the presence of large, unaffected Si and Mg particles that are common in such T6 heat-treated alloys [7].

Figure 1 shows also the $\alpha - Al$ cell microstructure for the AlSi7Mg0.6-DAA sample, which is composed of regularly distributed nanometric precipitates and contains dislocations. Observations allow to distinguish two types of nanoprecipitates: the smallest are needle-shaped precipitates that are elongated in the $[001]_{Al}$ direction. The larger nanometric precipitates are observed edge-on and are scattered in the microstructure, as shown in Figure 1. These precipitates do not appear to share a particular orientation with the aluminum matrix. Dislocations can be seen both within the cells and between the cells (in the inter-cell regions). Some dislocations appear to have interacted with the nanoprecipitates, as evidenced by the irregular lines shown in Figure 1.

On a general point of view, the impact of different ion-based preparation techniques on the observed microstructures can be compared in Figure 3. The use of a gallium ion beam (FIB, Figure 3 a. and b.) or an argon ion beam (PIPS, Figure 3 c.) on the sample results in homogeneous thinning of the $\alpha - Al$ and Si walls, indicating that both cellular walls and $\alpha - Al$ are polished in the same way. This assumption is supported by tilted TEM observations of the sample, which show no contrast variation due to local thickness superposition, not presented here. The darker contrasts observed on the TJE sample are no longer visible in these figures, implying that the 3D Si cellular structure thickness has been significantly reduced and the sample thickness has become more homogeneous. The mean diameter of Al-cells remains close to 500 nm, as observed in the TJE sample (Figure 1), attesting that the preparation techniques do not change the overall Si-structure. As a direct consequence of the reduced thickness, Si cell structure observation and characterization are easier on PIPS- and FIB-prepared samples.

The fine microstructure of the AlSi7Mg0.6-DAA alloy prepared with Room Temperature Focused Ion Beam (RT-FIB) is shown in Figure 3 a.. Different types of precipitates can be seen in this figure: small nanometric needle-like precipitates and platelet-like precipitates of various diameters. It is also possible to observe the remaining Si cell structure and dislocations. Nanometric needle-like precipitates can be evidenced by the presence of pinned dislocations, as shown in Figure 3 a.. These precipitates are oriented in the $< 001 >_{Al}$

directions. It is reasonable to assume that dislocations formed during the elaboration process were released during the direct artificial aging heat treatment and/or specimen thinning and were thus able to move through the nanoprecipitates array. Compared to the twin jet electropolished samples (Figure 1), the microstructure of the RT-FIB (Figure 3 a.) presents more platelet-like precipitates.

Platelet-like precipitates with diameters of about 100 nm can only be seen edge-on on $(100)_{Al}$ or $(010)_{Al}$ planes. Other platelet-like precipitates with diameters less than 50 nm have been observed in the $(001)_{Al}$ planes. The images displayed here represent the global microstructure.

The comparison of Figure 3 a. and b. illustrates the effect of preparation temperature on the microstructure. The Low Temperature FIB (LT-FIB, Figure 3 b.) preparation of the AlSi7Mg0.6-DAA microstructure exhibits significant distinctions from the RT-FIB preparation (Figure 3 a.). The nanoprecipitate found in the microstructure after RT-FIB appears to be thicker than that found in the LT-FIB sample, and platelet-like precipitates are less numerous within the microstructure. The needle-like precipitates are in the $< 100 >_{Al}$ directions for both preparation techniques considered here, and the platelet-like precipitates are in the $\{100\}_{Al}$ planes. The microstructure contains a few dislocations that are poorly resolved due to the sample orientation.

Figure 3 c. depicts the final microstructure investigated as a result of a room temperature PIPS preparation technique. In this case, several needle-like precipitates can be seen in the $< 100 >_{Al}$ directions. These needle-like precipitates are larger than those seen in Figure 1 when compared to the other preparation techniques. Only a few platelet-like precipitates have been observed without a specific habit plane. Many dislocations have been observed, sometimes interacting with needle-like precipitates.

Based on previous research [7, 24–27] it can be assumed that needle-like precipitates are β'' precipitates with the potential to evolve into $U1 - MgAl_2Si_2$ or $U2 - Mg_2Al_2Si_2$ for larger ones [24, 28]. Other precipitates observed could be of various types, as suggested by the precipitation sequence of the $\beta - Mg_2Si$ precipitates [11, 24, 29].

Discussion

Table 1 summarizes the influence of the preparation techniques on the observed microstructures: the size and type of precipitates are strongly influenced by the TEM sample preparation technique and appear to be directly related to the thermal history of the samples.

The microstructure of the material is not expected to evolve during electropolishing because a constant temperature of -30°C is used. On the contrary, samples are heated during ion beam thinning, and their exact thermal history is difficult to assess. The ion flux density is linked to the beam current, diameter, and acceleration voltage [30], and at a given acceleration voltage, gallium-ion influence is greater than argon-ion influence [31], owing to atom size and penetration depth. Moreover, Ga+ FIBs were used on average at higher acceleration voltages and currents than Ar+ PIPS for these preparation techniques. The beam diameter and sample size in FIB are both smaller than in PIPS, resulting in higher ion density and poorer energy dissipation. Also, ion milling, and particularly gallium milling, is known to cause significant damage to aluminum samples [32]. Finally, temperature affects ion damage by dissipating some incident energy, low temperature FIB causes fewer changes than room temperature FIB. The used preparation techniques can then be sorted in order of increasing ion damage: TJE, PIPS, LT-FIB and RT-FIB.

As it appears to be the best preparation technique for fine Al-cell microstructure observation, twin jet electropolishing was used on an over-artificially aged sample (Supplementary Figure). This enables the differentiation of thicker needle-like precipitates from platelet-like precipitates. There is an increase in the number of platelet-like precipitates. The results of the overaged sample (Direct Artificial Aged 2: DAA2, 210 °C / 30 minutes) are similar to those of the AlSi7Mg0.6-DAA alloys prepared with PIPS or FIB. As a result, the observed fine microstructure modification is primarily due to the increase in temperature during heat treatment.

Table 1. Summary of observations on the effect of preparation technique on the AlSi7Mg0.6 microstructure.

	Twin Jet Electropolishing	**Focused Ion Beam**		**Precision Ion Polishing System**
	Room Temperature	*Room Temperature*	*Low Temperature*	*Room Temperature*
Corresponding Figure / Precipitate morphology	Figure 1	Figure 3 a.	Figure 3 b.**Erreur ! Source du renvoi introuvable.**	Figure 3 c.**Erreur ! Source du renvoi introuvable.**
Needle-like (diameter lower than 10 nm)	Numerous	Some	Few	Some
Flake-like (diameter between 10 and 50 nm)	Few	Numerous	Numerous	Some
Platelet-like (over 50 nm)	Few	Numerous	Some	Not observed

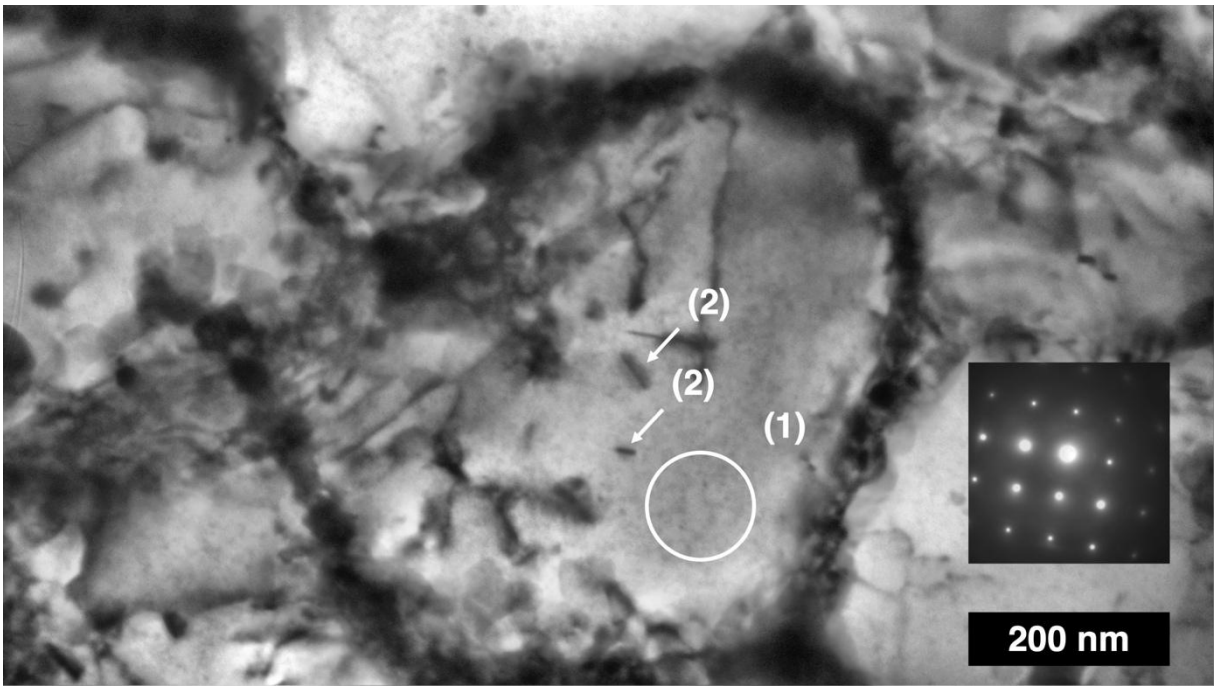

Figure 1. TEM micrograph of an AlSi7Mg0.6-Direct Aged Sample (DAA) prepared by Twin Jet Electropolishing in the $[001]_{Al}$ *direction. The corresponding Selected Area Electrons Diffraction (SAED) pattern is inserted into the image. With this preparation technique, cell walls appear with a dark contrast due to the local thickness. The intracellular microstructure is characterized by very small needle-like precipitates (1) and larger platelet-like ones (2).*

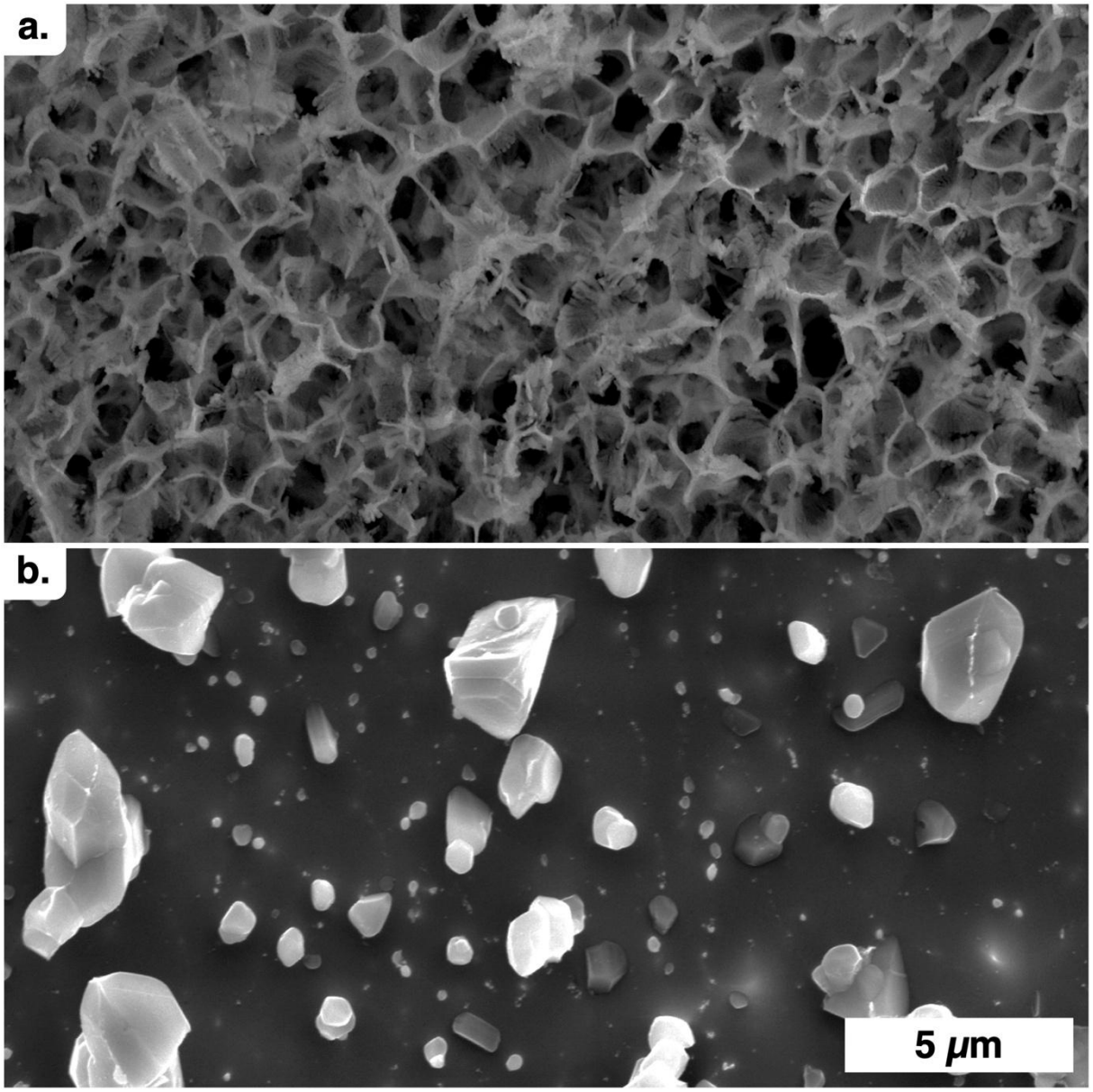

Figure 2. FEG-SEM observation of the surface of a twin jet electropolished AlSi7Mg0.6 DAA (a.) and heat treated optimized T6 (oT6) (b.) for TEM observation.

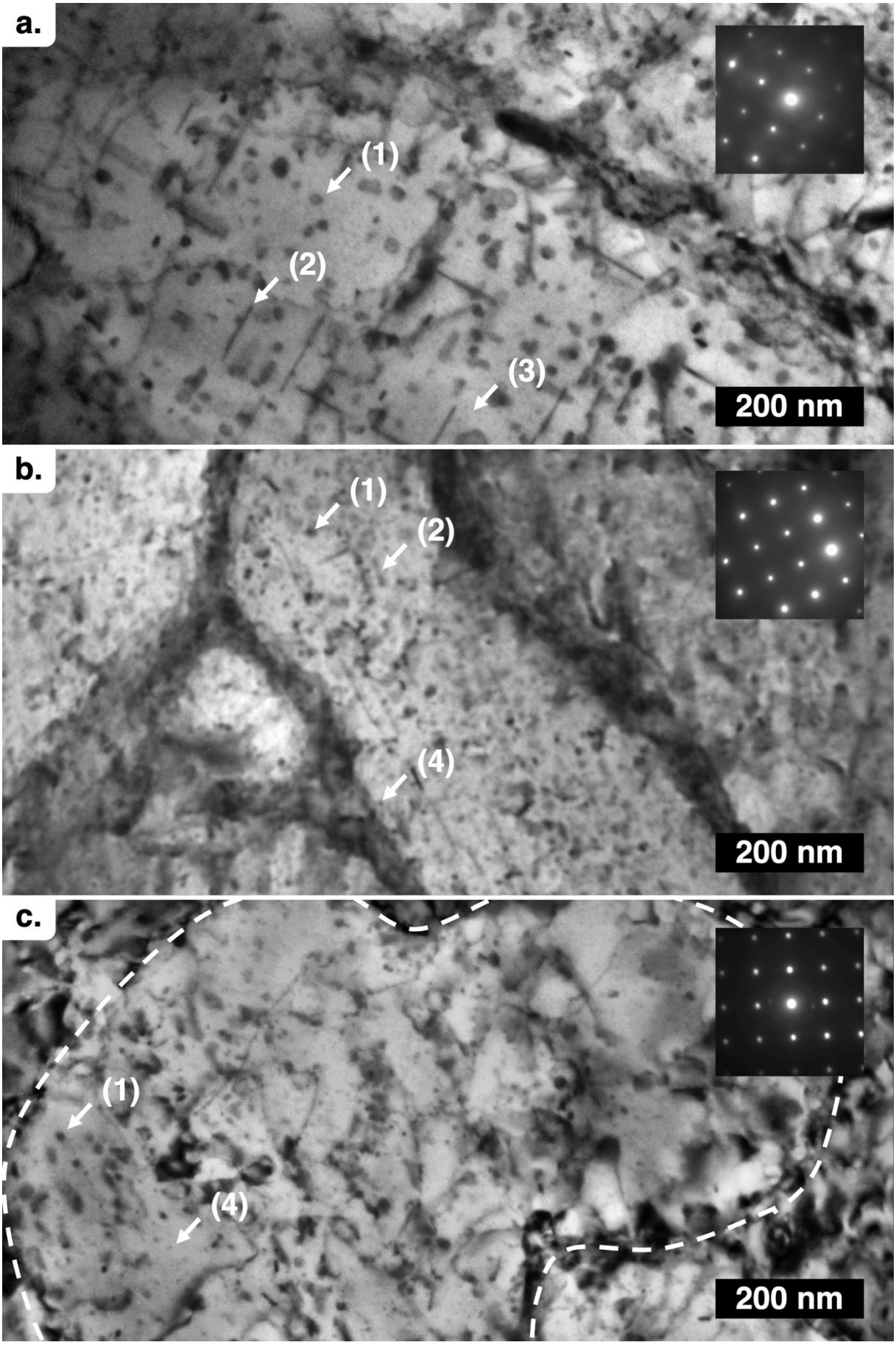
a.
(1)
(2)
(3)
200 nm
b.
(1)
(2)
(4)
200 nm
c.
(1)
(4)
200 nm

Figure 3. TEM observation of the AlSi7Mg0.6-DAA sample prepared with (a.) Room Temperature FIB, (b.) Low Temperature FIB and (c.) Room Temperature PIPS. On all figures, the Si-walls appear clearly with a reduced thickness with the presence of globular precipitates (1) as well as platelet-like ones (2). Smaller needle-like precipitates (3) or larger ones can be observed on the microstructures. All observations are taken alongside the $[001]_{Al}$ *direction with the associated SAED pattern inserted.*

Conclusions

The influence of the sample preparation on the AlSi7Mg0.6-DAA alloy transformed by laser beam melting, which presents a microstructure formed by $\alpha - Al$ cells embedded in a Si-rich network, has been investigated. Several issues have been raised:

- Twin jet electropolishing provides appropriate conditions for observing the fine microstructure of $\alpha - Al$ cells as it does not appear to significantly alter it. However, due to local over thickness, selective polishing is noticed, preventing accurate Si-rich network characterizations.
- PIPS and FIB ion milling techniques produce homogeneous sample thickness, making global material structure observations easier. Yet, modifications of precipitation characteristics in the cells are also observed and should be considered as it could skew results if precise and/or quantified characterizations (phases, sizes, proportion) are required.
- The observed changes are consistent with a local temperature increase during sample preparation, and result in the coarsening of the needle-like precipitates into larger or different ones, as predicted by the precipitation sequence. An influence of a local temperature increase is even observed for low temperature FIB.

The preparation technique should then be given special consideration: the microstructure characterization is strongly dependent on the energy introduced into the microstructure during sample preparation. However, using the same preparation technique will not affect the evolution of the observations of the microstructure resulting from two different thermal treatments.

Acknowledgments

This work has been conducted within the framework of The IRT Saint Exupery ANalysis of Defects and DURability Optimisation project (ANDDURO) sponsored by: Airbus, Airbus DS, Capgemini Engineering, CNRS, Daher, Element, Latecoere, Lauak, Liebherr, Laam, Mecaprotec, Oerlikon, Freyssinet Aero, Satys, Safran, Stelia, the national research agency (ANR) and the region Occitanie.

The authors would like to acknowledge the participation of Cécile Marcelot, Dominique Lamirault, Catherine Crestou, Robin Cours and Mariano Barrado Meléndez for their help in the TEM thin foil preparation.

Data Availability

The raw and processed data required to reproduce these findings cannot be shared at this time as the data also forms part of an ongoing study.

Conflict of interest

On behalf of all authors, the corresponding author states that there is no conflict of interest.

References

1. Santos Macías JG, Douillard T, Zhao L, et al (2020) Influence on microstructure, strength and ductility of build platform temperature during laser powder bed fusion of AlSi10Mg. Acta Mater 201:231–243. https://doi.org/10.1016/j.actamat.2020.10.001
2. Park T, Baek M, Hyer H, et al (2021) Effect of direct aging on the microstructure and tensile properties of AlSi10Mg alloy manufactured by selective laser melting process. Mater Charact 176:111113. https://doi.org/10.1016/j.matchar.2021.111113
3. Dong Z, Xu M, Guo H, et al (2022) Microstructural evolution and characterization of AlSi10Mg alloy manufactured by selective laser melting. Journal of Materials Research and Technology 17:2343–2354. https://doi.org/10.1016/j.jmrt.2022.01.129
4. Takata N, Liu M, Kodaira H, et al (2020) Anomalous strengthening by supersaturated solid solutions of selectively laser melted Al–Si-based alloys. Addit Manuf 33:101152. https://doi.org/10.1016/j.addma.2020.101152
5. Měsíček J, Čegan T, Ma Q, et al (2022) Effect of artificial aging on the strength, hardness, and residual stress of SLM AlSi10Mg parts prepared from the recycled powder. Materials Science and Engineering: A 855:143900. https://doi.org/10.1016/j.msea.2022.143900
6. Albu M, Krisper R, Lammer J, et al (2020) Microstructure evolution during in-situ heating of AlSi10Mg alloy powders and additive manufactured parts. Addit Manuf 36:101605. https://doi.org/10.1016/j.addma.2020.101605
7. Galy C, Bello N, Larignon C, Perusin S (2021) Research of Specific Heat Treatment for AlSi7Mg0.6 Alloy Manufactured by Laser Beam Melting. In: Metal Powder Industries Federation (ed) Advances in Additive Manufacturing with Powder Metallurgy. Compiled By: Sundar Atre & Stuart Jackson, Princeton, pp 185–197
8. Takata N, Kodaira H, Sekizawa K, et al (2017) Change in microstructure of selectively laser melted AlSi10Mg alloy with heat treatments. Materials Science and Engineering A 704:218–228. https://doi.org/10.1016/j.msea.2017.08.029
9. Aboulkhair NT, Maskery I, Tuck C, et al (2016) The microstructure and mechanical properties of selectively laser melted AlSi10Mg: The effect of a conventional T6-like heat treatment. Materials Science and Engineering A 667:139–146. https://doi.org/10.1016/j.msea.2016.04.092
10. Yang K v., Rometsch P, Davies CHJ, et al (2018) Effect of heat treatment on the microstructure and anisotropy in mechanical properties of A357 alloy produced by selective laser melting. Mater Des 154:275–290. https://doi.org/10.1016/j.matdes.2018.05.026
11. Zhou L, Mehta A, Schulz E, et al (2018) Microstructure, precipitates and hardness of selectively laser melted AlSi10Mg alloy before and after heat treatment. Mater Charact 143:5–17. https://doi.org/10.1016/j.matchar.2018.04.022

12. Qin H, Dong Q, Fallah V, Daymond MR (2020) Rapid Solidification and Non-equilibrium Phase Constitution in Laser Powder Bed Fusion (LPBF) of AlSi10Mg Alloy: Analysis of Nano-precipitates, Eutectic Phases, and Hardness Evolution. Metallurgical and Materials Transactions A 51:448–466. https://doi.org/10.1007/s11661-019-05505-5

13. Salandari-Rabori A, Diak BJ, Fallah V (2022) Dislocation-obstacle interaction evolution in rate dependent plasticity of AlSi10Mg as-built microstructure by laser powder bed fusion. Materials Science and Engineering: A 857:144043. https://doi.org/10.1016/j.msea.2022.144043

14. Tang H, Gao C, Zhang Y, et al (2023) Effects of direct aging treatment on microstructure, mechanical properties and residual stress of selective laser melted AlSi10Mg alloy. J Mater Sci Technol 139:198–209. https://doi.org/10.1016/j.jmst.2022.08.032

15. Fousová M, Dvorský D, Michalcová A, Vojtěch D (2018) Changes in the microstructure and mechanical properties of additively manufactured AlSi10Mg alloy after exposure to elevated temperatures. Mater Charact 137:119–126. https://doi.org/10.1016/j.matchar.2018.01.028

16. Lefebvre W, Rose G, Delroisse P, et al (2021) Nanoscale periodic gradients generated by laser powder bed fusion of an AlSi10Mg alloy. Mater Des 197:109264. https://doi.org/10.1016/j.matdes.2020.109264

17. Fite J, Eswarappa Prameela S, Slotwinski JA, Weihs TP (2020) Evolution of the microstructure and mechanical properties of additively manufactured AlSi10Mg during room temperature holds and low temperature aging. Addit Manuf 36:101429. https://doi.org/10.1016/j.addma.2020.101429

18. Hadadzadeh A, Amirkhiz BS, Mohammadi M (2019) Contribution of Mg2Si precipitates to the strength of direct metal laser sintered AlSi10Mg. Materials Science and Engineering A 739:295–300. https://doi.org/10.1016/j.msea.2018.10.055

19. Ruffilli R (2017) Fatigue mechanisms in Al-based metallizations in power MOSFETs

20. Fiocchi J, Tuissi A, Biffi CA (2021) Heat treatment of aluminium alloys produced by laser powder bed fusion: A review. Mater Des 204:. https://doi.org/10.1016/j.matdes.2021.109651

21. Akula SP, Ojha M, Rao KL, Gupta AK (2023) A review on superplastic forming of Ti-6Al-4V and other titanium alloys. Mater Today Commun 34:105343. https://doi.org/10.1016/j.mtcomm.2023.105343

22. Titus D, James Jebaseelan Samuel E, Roopan SM (2019) Nanoparticle characterization techniques. In: Green Synthesis, Characterization and Applications of Nanoparticles. Elsevier, pp 303–319

23. Gupta AK, Lloyd DJ, Court SA (2001) Precipitation hardening processes in an alloy Al-0.4%Mg-1.3%Si-0.25%Fe aluminum alloy. Materials Science and Engineering A 301:140–146. https://doi.org/10.1016/S0921-5093(00)01814-1

24. Ding L, Jia Z, Nie JF, et al (2018) The structural and compositional evolution of precipitates in Al-Mg-Si-Cu alloy. Acta Mater 145:437–450. https://doi.org/10.1016/j.actamat.2017.12.036

25. Zandbergen HW, Andersen SJ, Jansen J (1997) Structure determination of Mg5Si6 particles in Al by dynamic electron diffraction studies. Science (1979) 277:1221–1225. https://doi.org/10.1126/science.277.5330.1221

26. Andersen SJ, Marioara CD, Vissers R, et al (2007) The structural relation between precipitates in Al-Mg-Si alloys, the Al-matrix and diamond silicon, with emphasis on the trigonal phase U1-MgAl2Si2. Materials Science and Engineering A 444:157–169. https://doi.org/10.1016/j.msea.2006.08.084

27. Andersen SJ, Zandbergen HW, Jansen J, et al (1998) The crystal structure of the β″ phase in Al-Mg-Si Alloys. Acta Mater 46:3283–3298. https://doi.org/10.1016/S1359-6454(97)00493-X

28. Vissers R, van Huis MA, Jansen J, et al (2007) The crystal structure of the β′ phase in Al-Mg-Si alloys. Acta Mater 55:3815–3823. https://doi.org/10.1016/j.actamat.2007.02.032

29. Edwards GA, Stiller K, Dunlop GL, Couper MJ (1998) The precipitation sequence in Al-Mg-Si alloys. Acta Mater 46:3893–3904. https://doi.org/10.1016/S1359-6454(98)00059-7

30. Mitrofanov MI, Voznyuk G v., Rodin SN, et al (2020) Calculation of the Ga+ FIB Ion Dose Distribution by SEM Image. Semiconductors 54:1682–1684. https://doi.org/10.1134/S1063782620120246

31. Ryabkina X, Stepanova O (2014) Calculation of Energy Release Function of Ion Beam in Solids. Adv Mat Res 880:7–12. https://doi.org/10.4028/www.scientific.net/AMR.880.7

32. Unocic KA, Mills MJ, Daehn GS (2010) Effect of gallium focused ion beam milling on preparation of aluminium thin foils. J Microsc 240:227–238. https://doi.org/10.1111/j.1365-2818.2010.03401.x